Cyclic Nucleotide–gated Channels Colocalize with Adenylyl Cyclase in Regions of Restricted cAMP Diffusion

Thomas C. Rich,* Kent A. Fagan,‡ Hiroko Nakata,‡ Jerome Schaack,§ Dermot M.F. Cooper,‡ and Jeffrey W. Karpen*

From the *Department of Physiology and Biophysics, ‡Department of Pharmacology, and §Department of Microbiology, University of Colorado Health Sciences Center, Denver, CO 80262

abstract Cyclic AMP is a ubiquitous second messenger that coordinates diverse cellular functions. Current methods for measuring cAMP lack both temporal and spatial resolution, leading to the pervasive notion that, unlike Ca^{2+}, cAMP signals are simple and contain little information. Here we show the development of adenovirus-expressed cyclic nucleotide–gated channels as sensors for cAMP. Homomultimeric channels composed of the olfactory α subunit responded rapidly to jumps in cAMP concentration, and their cAMP sensitivity was measured to calibrate the sensor for intracellular measurements. We used these channels to detect cAMP, produced by either heterologously expressed or endogenous adenylyl cyclase, in both single cells and cell populations. After forskolin stimulation, the endogenous adenylyl cyclase in C6-2B glioma cells produced high concentrations of cAMP near the channels, yet the global cAMP concentration remained low. We found that rapid exchange of the bulk cytoplasm in whole-cell patch clamp experiments did not prevent the buildup of significant levels of cAMP near the channels in human embryonic kidney 293 (HEK-293) cells expressing an exogenous adenylyl cyclase. These results can be explained quantitatively by a cell compartment model in which cyclic nucleotide–gated channels colocalize with adenylyl cyclase in microdomains, and diffusion of cAMP between these domains and the bulk cytosol is significantly hindered. In agreement with the model, we measured a slow rate of cAMP diffusion from the whole-cell patch pipette to the channels (90% exchange in 194 s, compared with 22–56 s for substances that monitor exchange with the cytosol). Without a microdomain and restricted diffusional access to the cytosol, we are unable to account for all of the results. It is worth noting that in models of unrestricted diffusion, even in extreme proximity to adenylyl cyclase, cAMP does not reach high enough concentrations to substantially activate PKA or cyclic nucleotide–gated channels, unless the entire cell fills with cAMP. Thus, the microdomains should facilitate rapid and efficient activation of both PKA and cyclic nucleotide–gated channels, and allow for local feedback control of adenylyl cyclase. Localized cAMP signals should also facilitate the differential regulation of cellular targets.

key words: intracellular signaling • cyclic AMP • calcium influx • microdomains • subcellular compartments

INTRODUCTION

The second messenger cyclic AMP (cAMP) regulates a large variety of cellular processes including Ca^{2+} influx (Tsien, 1983; Trautwein and Hescheler, 1990; Frings et al., 1995; Finn et al., 1996), cellular excitability (Levitan, 1994; Gray et al., 1998), and gene expression (Montminy, 1997), yet little is known about the spatial and temporal features of cAMP signals. The highest resolution method for measuring cAMP in single cells relies on fluorescence resonance energy transfer between labeled subunits of cAMP-dependent protein kinase (PKA) (Adams et al., 1991; Zaccolo et al., 2000). This ingenious method allows the detection of changes in cAMP throughout the cytosol. However, the reassociation of labeled PKA subunits is slow, due in part to the redistribution of labeled catalytic subunits into different cellular compartments (Harootunian et al., 1993). Furthermore, the method cannot measure localized changes in cAMP. Rather than modify this method, we chose a novel approach, measuring cAMP-induced currents through heterologously expressed rat olfactory cyclic nucleotide–gated (oCNG)[1] channels (Dhallan et al., 1990).

The endogenous cyclic nucleotide–gated channels in retinal rods have been used as a high-resolution monitor of cGMP signaling. These measurements have led to quantitative descriptions of the single photon response (Baylor et al., 1979), the cGMP concentration responsible for the dark current (Nakatani and Yau, 1988), and the characterization of the interplay between guanylyl cyclase and cGMP-specific phosphodiesterase (PDE) in reg-

[1]*Abbreviations used in this paper:* AC, adenylyl cyclase; AKAP, A-kinase anchoring protein; HEK, human embryonic kidney; NPE-cAMP, 1-(2-nitrophenyl)ethyl-cAMP; oCNG channel, olfactory cyclic nucleotide-gated channel; PDE, phosphodiesterase.

ulating cGMP levels (Koutalos et al., 1995b,c). These channels have also been used in conjunction with optical methods to measure the reduction in the diffusion coefficient for cGMP due to baffling by the disks and buffering of cGMP (Lamb et al., 1981; Cameron and Pugh, 1990; Olson and Pugh, 1993; Koutalos et al., 1995a,d; Gray-Keller et al., 1999). Overall, these studies have complemented and extended biochemical studies of phototransduction and, as such, have allowed an unprecedented view of feedback control within a second messenger signaling pathway (Stryer, 1991; Lagnado and Baylor, 1992; Pugh and Lamb, 1993; Yarfitz and Hurley, 1994; Yau, 1994; Polans et al., 1996; Pugh et al., 1997; Molday, 1998).

Studies using endogenous cyclic nucleotide–gated channels have been limited to only a few other cell types, including olfactory receptors (Detlev and Restrepo, 1998; Gold, 1999), and neurons of the marine opisthobranch snail, *Pleurobranchaea californica* (Sudlow and Gillette, 1997). In many cases, findings in such highly specialized cell types are not easily extended to cells with different signaling molecules and diverse feedback mechanisms. For example, nine isoforms of adenylyl cyclase (AC) are differentially regulated by a variety of cellular signaling molecules, including G proteins, Ca^{2+}, PKA, PKC, and CaM kinase (Smit and Iyengar, 1998). Similarly, the isoforms of phosphodiesterase are differentially regulated by intracellular signals (Beavo, 1995). Thus, to understand the diversity of cAMP signaling, a generally applicable method to measure cAMP concentrations is required.

Recently, cyclic nucleotide–gated channels have been artificially introduced into other cell types using the "patch-cramming" technique (Trivedi and Kramer, 1998). This technique uses excised, inside-out macropatches containing channels "crammed" into recipient cells to measure cytosolic cyclic nucleotide concentrations near the tip of the pipette. As such, this method is well-suited to study cyclic nucleotides produced within the cytosol (e.g., by soluble guanylyl cyclase) of large cells. In contrast, we have incorporated oCNG channels in the surface membrane where AC is known to reside (Krupinski et al., 1989). This method is ideally suited to studying the membrane-localized, cAMP-signaling pathways. Further, we used adenovirus constructs encoding the oCNG channel to allow expression in a variety of cell types. Surprisingly, using this approach, we discovered that oCNG channels and AC colocalize within regions of restricted cAMP diffusion.

MATERIALS AND METHODS

Cell Culture and Expression

Both human embryonic kidney 293 (HEK-293) cells and HEK-293 cells stably expressing type 8 AC (HEK-AC8) were maintained in 10 ml of MEM (Life Technologies) with 10% vol/vol fetal bovine serum (Gemini) and 0.1 mg/ml G418, and grown in 75 cm² flasks

at 37°C in a humidified atmosphere of 95% air/5% CO_2. Cells were plated at ~60% confluence in 100-mm culture dishes for infection with the oCNG channel-encoding adenovirus construct (Fagan et al., 1999; multiplicity of infection = 10). 2 h after infection, hydroxyurea was added to the cell media at 2 mM final concentration to inhibit viral replication. C6-2B cells were maintained as described previously (Fagan et al., 1999). HEK-AC8 (24 h after infection) and C6-2B cells (48–72 h after infection) were detached with phosphate-buffered saline containing 0.03% EDTA, resuspended in serum-containing media, and assayed within 12 h.

Electrical Recording

Recordings were made at room temperature (19–21°C) using an Axopatch-200A patch-clamp amplifier (Axon Instruments, Inc.) and whole-cell, perforated patch, and excised patch techniques. Pipettes were pulled from borosilicate glass and heat polished. Pipettes were lowered onto the cells and gigaohm seals were formed (8.3 ± 3.3 GΩ). Pipette resistance was limited to 5 MΩ and averaged 3.4 ± 1.0 MΩ. Current records were typically sampled at five times the filter setting and stored on an IBM compatible computer. Records were corrected for errors due to series resistance. Unless otherwise noted, all data are presented as mean $\pm$ SD. The solution within the chamber (100 µl) was changed within 15 s using a gravity-driven perfusion system.

Whole-cell and perforated patch configurations. After achieving whole-cell or perforated patch configuration, capacitive transients were elicited by applying 20-mV steps from the holding potential and recorded at 40 kHz (filtered at 10 kHz) for calculation of access resistance. In the whole-cell configuration, the access resistance averaged 6.6 ± 3.1 MΩ. No significant difference in access resistance was observed in whole-cell experiments performed under different experimental conditions. Access resistance was monitored throughout the experiments to ensure stable electrical access was maintained. The solutions used for all of the experiments are listed in Table I. Whole-cell pipette solution 1 (Table I) was used as the control solution for all whole-cell experiments. In the perforated patch configuration, pipette solutions (perforated patch 1 and 2, Table I) contained nystatin (diluted from 50 mg/ml stock in dimethylsulfoxide) to gain electrical access to the cell. These solutions were kept on ice and shielded from light until use. A steady access resistance (15–60 MΩ) was obtained 5–15 min after seal formation. Nystatin did not induce measurable currents up to 20 min after break-in in whole-cell experiments. Voltage protocols were selected to minimize endogenous currents.

Excised, inside-out patch configuration. Excised patch solution (Table I) was used in both the pipette and bath. Cyclic AMP was added to the bath solution in concentrations between 1 and 1,000 µM. cAMP-induced currents were obtained from the difference between currents in the presence and absence of cAMP.

Photolysis of NPE-cAMP

The response of oCNG channels to flash photolysis of NPE-cAMP was measured in the whole-cell patch-clamp configuration. The pipette filling solution (whole-cell pipette 2 or 3, Table I) was kept on ice and shielded from light until use. After achieving whole-cell configuration, we waited 10 min before photolysis of NPE-cAMP. Photolysis of NPE-cAMP was achieved by direct flash (1 ms) of the entire bath with an XF-10 xenon flashlamp (HI-TECH Scientific). The DMSO used to dissolve NPE-cAMP and nystatin ($\leq$0.5% final concentration) had no effect on channels in excised patches.

Determination of Total cAMP in C6-2B Cells

C6-2B cells were suspended in low-Mg bath 1 solution (Table I) for 10 min at 20°C. cAMP accumulation was initiated by addition

Solution	NaCl	KCl	K-gluconate	MgCl$_2$	d-Glucose	HEPES	K$_2$ATP	Nystatin	cAMP	pCPT-cGMP*	NPE-cAMP‡	IBMX§	RO 20-1724‖	EGTA	EDTA
High-Mg Bath 1	140	4	0	10	11	10	0	0	0	0	0	0	0	0	0
Low-Mg Bath 1	140	4	0	0.1	11	10	0	0	0	0	0	0	0	0	0
High-Mg Bath 2	140	4	0	10	11	10	0	0	0	0	0	0.5	0.01	0	0
Low-Mg Bath 2	140	4	0	0.1	11	10	0	0	0	0	0	0.5	0.01	0	0
Excised Patch	130	0	0	0	0	3	0	0	0	0	0	0	0	1	0.02
Whole-cell Pipette 1	4	140	0	0.5	0	10	0	0	0	0	0	0	0	0	0
Whole-cell Pipette 2	4	140	0	0.5	0	10	0	0	0.02	0	0.2	0	0	0	0
Whole-cell Pipette 3	4	140	0	0.5	0	10	0	0	1	0	0.2	0	0	0	0
Whole-cell Pipette 4	4	140	0	0.5	0	10	5	0	0	0	0	0	0	0	0
Whole-cell Pipette 5	140	4	0	0.5	0	10	0	0	0	0	0	0	0	0	0
Whole-cell Pipette 6	4	140	0	0.5	0	10	0	0	0.04	0	0	0.5	0.01	0	0
Whole-cell Pipette 7	4	140	0	0.5	0	10	0	0	1	0	0	0.5	0.01	0	0
Whole-cell Pipette 8	4	140	0	0.5	0	10	0	0	0	$5*10^{-4}$	0	0	0	0	0
Perforated Patch 1	4	70	70	0.5	0	10	0	0.04–0.2	1	0	0	0	0	0	0
Perforated Patch 2	4	70	70	0.5	0	10	0	0.04–0.2	0	0	0	0	0	0	0

All concentrations are in millimolar. Solutions were pH 7.4 except the excised-patch solution, which was pH 7.6. *8-*p*-chlorophenylthio-cGMP, ‡1-(2-nitrophenyl)ethyl-cAMP, §3-isobutyl-1-methylxanthine, ‖4-(3-butoxy-4-methoxybenzyl)-2-imidazolidinone.

of forskolin or vehicle for 2.5 min and terminated by addition of trichloroacetic acid (9% wt/vol). The total intracellular levels of cAMP were measured by a cAMP binding assay (Amersham Pharmacia Biotech) as previously described (Boyajian et al., 1991). The sample cAMP content was calculated from a standard curve. Cellular concentration was estimated assuming that the accessible cell volume was the aqueous volume fraction (0.9) of the total cell volume. The total cell volume was measured by (a) counting the number of cells in a fixed volume, (b) pelleting a known number of cells, and (c) measuring the packed volume of the pellet. The cells were approximately spherical in suspension, yielding a mean radius of 8.4 μm. The results represent mean ± SEM performed in triplicate.

Measurement of Ca^{2+}

Intracellular [Ca^{2+}] was measured in cell populations using fura-2 as the Ca^{2+} indicator, as previously described (Boyajian et al., 1991; Fagan et al., 1999). Free Ca^{2+} concentrations were estimated using $[Ca^{2+}] = K_d \times f \times (R - R_{min})/(R_{max} - R_{min})$, where K_d, R, R_{min}, R_{max}, and f have their usual meanings.

Forskolin was from Calbiochem. Fura-2/AM, Pluronic F-127, and NPE-cAMP were from Molecular Probes. All other chemicals were from Sigma-Aldrich.

R E S U L T S

Cyclic nucleotide–gated channels have the following properties that led us to investigate their utility as cAMP sensors. First, oCNG channels can be expressed easily in a variety of cell types using a recently described adenovirus construct encoding the α subunit (Fagan et al., 1999). Second, several hundred channels provide a readily detectable readout of cAMP concentration without significantly buffering the cAMP signal being measured. Third, cyclic nucleotide–gated channels respond rapidly to changes in cyclic nucleotide concentration (Karpen et al., 1988; Hagen et al., 1996). Fourth, the sensor can be calibrated in different cell types by measuring the apparent cAMP affinity in excised mem-

brane patches. This controls for the possible modulation of oCNG channels by endogenous proteins.

Response of oCNG Channels to Jumps in cAMP

The response times of homomultimeric oCNG channels to changes in cAMP have not been established. We examined the ionic currents induced by perturbations in cellular cAMP levels generated by photolysis of a "caged" cAMP analogue, NPE-cAMP. oCNG channels were expressed in the HEK-AC8 cell line and currents were monitored using the whole-cell patch-clamp technique. The pipette solution (whole-cell pipette 2, Table I) contained 200 μM NPE-cAMP and 20 μM cAMP to verify that there was channel activity, and to prime the channels to give a larger flash response. The bath solution initially contained 0.1 mM $MgCl_2$ (low-Mg bath 1, Table I) to allow measurement of inward current through oCNG channels at a membrane potential of −50 mV. After a 1-ms flash, there was a brief delay, 14.8 ± 4.1 ms ($n = 4$), followed by an exponential increase in current, $\tau = 212 \pm 53$ ms (Fig. 1 A). This current was subsequently blocked by 10 mM $MgCl_2$ (high-Mg bath 1, Table I) and, in the continued presence of 10 mM $MgCl_2$, repeated photolysis of NPE-cAMP did not induce a detectable inward current (Fig. 1 A). When the external $MgCl_2$ concentration was returned to 0.1 mM, current through oCNG channels was no longer blocked and could again be induced by photolysis of NPE-cAMP. No currents were induced by the photolysis of NPE-cAMP when 1 mM cAMP (a supersaturating concentration) was added to the pipette solution (whole-cell pipette 3, Table I) or in control cells not infected with the oCNG-encoding adenovirus construct (Fig. 1 B). The kinetics of the cAMP-induced current were similar to the photolysis rate of NPE-cAMP (~4 s^{-1} at pH = 7.4), indicating that the photolysis rate of NPE-cAMP was the rate-limiting step in the response (Wootton and Trentham, 1989; Lowe and Gold, 1993) and confirming that oCNG channels can indeed detect rapid changes in cAMP concentration.

Calibration of the Sensor

We determined the apparent cAMP affinity of oCNG channels in excised, inside-out patches from HEK-AC8 cells. After patch excision, currents were elicited by applying solutions containing between 0 and 1,000 μM cAMP at membrane potentials (V_m) of +50 and −50 mV. In excised patches expressing oCNG channels, increasing cAMP concentration induced larger currents until a saturating cAMP concentration was reached (Fig. 2 A). No cAMP-inducible current was observed in control cells. The sensitivity of oCNG channels to cAMP (Fig. 2 B) was quantified using the Hill equation (Fig. 2, legend), yielding an average apparent affinity ($K_{1/2}$) and Hill coefficient (N) of 40 ± 13 μM and 2.1 ± 0.2 (mea-
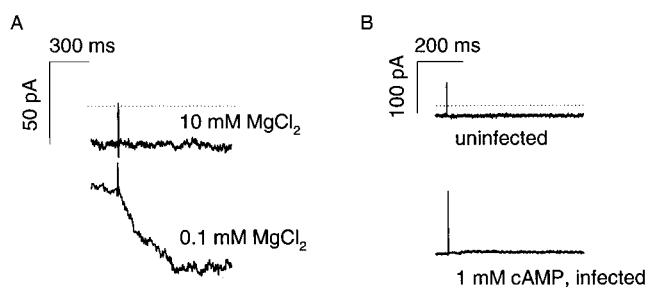

Figure 1. Response of oCNG channels expressed in an HEK-AC8 cell to the photolysis of caged cAMP. (A) Photolysis of NPE-cAMP is indicated by flash artifacts, $V_m = -50$ mV. Data are from one cell; the external solution contained either 0.1 or 10 mM $MgCl_2$. No photolysis-induced currents were observed when the cell was bathed in 10 mM $MgCl_2$. Zero current is indicated by the dotted line. The basal current was due to 20 μM cAMP in the pipette solution and a small amount of leak (see 10 mM $MgCl_2$ trace). (B) No response to the photolysis of caged cAMP was observed in cells not expressing oCNG channels (uninfected) or in oCNG channel–expressing cells with 1 mM cAMP added to the pipette solution.

sured at −50 mV, $n = 23$), similar to previously reported values for channels expressed in HEK-293 cells (Liu et al., 1994). These parameters were insensitive to changes in membrane potential (at +50 mV, $K_{1/2} = 41 \pm 15$ μM, $N = 2.2 \pm 0.3$, in the same 23 patches). To determine whether either the apparent affinity or Hill coefficient were modified as a result of patch excision, patches were excised directly into solutions containing a subsaturating cAMP concentration (Fig. 2 C). Upon patch excision, average current levels did not change over 30 min ($n = 4$). A further verification of the calibration in the whole-cell setting is presented later. These results demonstrate that, given the maximal current, the cAMP concentration can be readily calculated from measured currents and that the uncertainty in the cAMP concentrations can be estimated by the variability of the apparent affinity and the Hill coefficient. For example, if the fraction of maximal current (I/I_{max}) were found to be 0.6, the estimated cAMP concentration would be 49 ± 14 μM (Fig. 2 B). The concentrations that can be measured reliably using the wild-type channel are 10–100 μM.

Single Cell Measurement of cAMP Using oCNG Channels

To determine whether heterologously expressed oCNG channels could detect cAMP in single cells, we chose to first examine cAMP accumulation in the HEK-AC8 cell line. Adenylyl cyclase activity was stimulated with 50 μM forskolin[2] (added to low-Mg bath 1 solution, Table I)

---

[2]The forskolin concentrations used in this study were similar to those used in other studies (10–50 μM; Adams et al., 1991; Debernardi et al., 1993; Frace et al., 1993; DeBernardi and Brooker, 1996; Jurevicius and Fischmeister, 1996). These stimulus conditions may result in higher cAMP levels than would occur under more physiologic conditions. However, we did not maximally stimulate AC, nor did we inhibit phosphodiesterase activity (except for the data presented in Fig. 8).
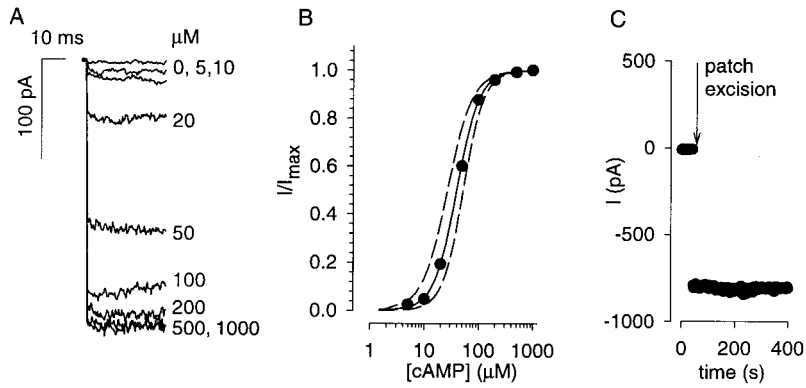
Figure 2. Dose response of oCNG channels expressed in HEK-AC8 cells. (A) Current traces in an excised, inside-out patch in response to increasing cAMP concentration. Currents were elicited by steps to -50 mV. (B) Dose-response relations fit with the Hill equation: $I/I_{max} = [cAMP]^N/([cAMP]^N + K_{1/2}^N)$. The data are from the experiment shown ($\bullet$), the average of 23 experiments (solid line) $\pm$ SD in $K_{1/2}$ and N (dashed lines). (C) Currents elicited by excising a patch directly into a solution containing 50 μM cAMP (a subsaturating concentration). No modulation of oCNG channel currents due to patch excision was observed.

and the subsequent activation of oCNG channels was monitored using the perforated patch technique (Horn and Marty, 1988; Zhou and Neher, 1993). In this configuration, the pore-forming antibiotic nystatin is included in the pipette solution to gain electrical access to the cell's interior, but divalent cations and larger molecules like cAMP are retained in the cell. The pipette solution (perforated patch 1, Table I) also contained supersaturating cAMP (1 mM) to measure the maximal current at the end of each experiment after rupture of the patch membrane (whole-cell configuration). After stimulation with forskolin, there was a brief delay followed by a steady increase in current that plateaued in $\sim$150 s (Fig. 3 A). In the presence of 0.1 mM external $MgCl_2$, the forskolin-induced current displayed little rectification. Subsequent addition of 10 mM $MgCl_2$ rapidly blocked the current, yielding a small outwardly rectifying current and confirming that this current was through oCNG channels (Fig. 3 B). The magnitude of the plateau current relative to the maximal current indicates that 55 $\pm$ 13 μM ($n = 5$) cAMP was produced (Fig. 3 C). The plateau likely reflects a balance between cAMP production, diffusion, degradation, and perhaps binding to proteins and extrusion. No forskolin-induced increase in current was observed in cells not expressing oCNG channels. Further, forskolin did not induce currents in excised patches containing oCNG channels (data not shown), indicating that forskolin is not an agonist of these channels.

To ensure that the high cAMP concentration measured by the channel was not due to the heterologous expression of AC in the HEK-AC8 cell line, we also examined the generation of cAMP by the endogenous type 6 AC in C6-2B glioma cells (Debernardi et al., 1993). Upon stimulation with 50 μM forskolin, there was a delay followed by a steady increase in current (Fig. 3 D). This current was subsequently blocked by 10 mM external $MgCl_2$. The ratio of the maximal forskolin-induced current to the maximal oCNG current indicates that the channel detected 42 $\pm$ 11 μM cAMP ($n = 3$, Fig. 3 E).

This concentration is far higher than the low micromolar levels of cAMP measured under the same stimulus conditions in single C6-2B cells using fluorescently labeled PKA subunits (DeBernardi and Brooker, 1996, 1998). Low cAMP levels have also been observed in single BC3H1 cells, in response to 50 μM forskolin (Adams et al., 1991). These results using the fluorescently labeled PKA method were consistent with earlier measures of cAMP in population assays in C6-2B and WI-38 cells (Barber and Butcher, 1980; Barovsky et al., 1983). To verify that our C6-2B cells were behaving normally, we measured total cellular cAMP using a binding assay (Fig. 3 F). When stimulated by 50 μM forskolin for 150 s, the total cAMP levels reached $\sim$4 μM, averaged over the cytosolic volume. It is important to note that this is very likely to be an overestimate of free cytosolic cAMP for two reasons: the measurement includes both free and bound cAMP, and it includes cAMP from all cellular compartments (including the diffusionally restricted microdomain). Further evidence that this assay overestimates free cAMP is that the measured basal level (2 μM) would saturate endogenous PKA activity, which is inconsistent with several studies in these same cells (Allen et al., 1998; Tian et al., 1998a,b). Importantly, all of the above measures are significantly less than the $\sim$25 μM detected by the channels at 150 s. Thus, the local cAMP concentration detected by oCNG channels was much higher (likely >12-fold) than the average cytosolic concentration. This suggests that oCNG channels colocalize with AC and that diffusion away from this region is hindered.

cAMP Accumulates Despite Rapid Dialysis of the Bulk Cytosol

If cAMP is generated in diffusionally limited microdomains, then forskolin-induced cAMP accumulation should be detectable in the whole-cell configuration in which there is rapid exchange of the bulk cytoplasm (with whole-cell pipette solution 4, Table I). We tested this prediction using HEK-AC8 cells expressing oCNG channels. After stimulation of AC with 50 μM forskolin, a steady rise to substantial current levels was observed
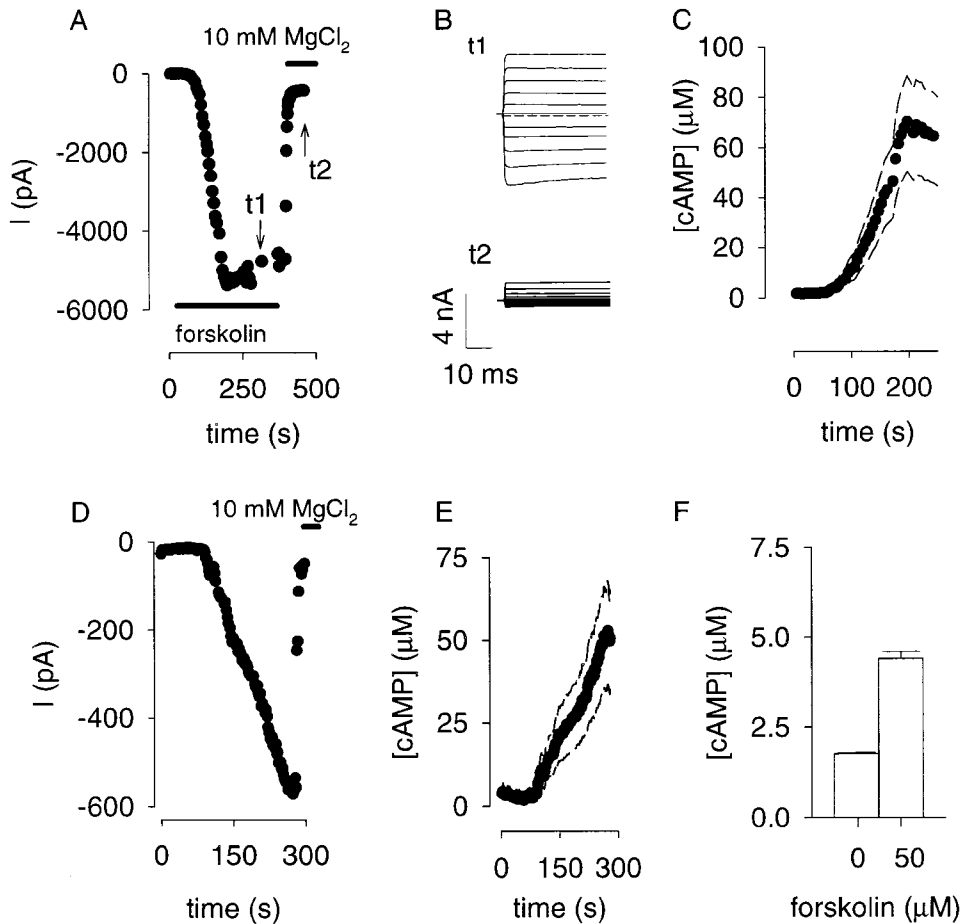
Figure 3. cAMP measurements in single cells expressing oCNG channels. (A) Forskolin-induced current in an HEK-AC8 cell, measured in perforated patch configuration, $V_m = -50$ mV. 50 μM forskolin and 10 mM MgCl$_2$ were applied as indicated. $I_{max} = 7{,}490$ pA. (B) Block of forskolin-induced currents at potentials between $+50$ and -50 mV (10-mV increments). The bath solution contained either 0.1 or 10 mM MgCl$_2$ at times t1 and t2, as indicated in A. (C) [cAMP] calculated using the Hill equation ($\bullet$) $\pm$ SD (dashed lines). (D) Response of a C6-2B cell to 50 μM forskolin (applied at time = 0), $V_m = -60$ mV. $I_{max} = 910$ pA. The response reached a plateau in $\sim$270 s. No forskolin-induced currents were observed in uninfected cells (cells not expressing oCNG channels). (E) [cAMP] calculated using the Hill equation ($\bullet$) $\pm$ SD (dashed lines). (F) Estimate of total [cAMP] in C6-2B cells.
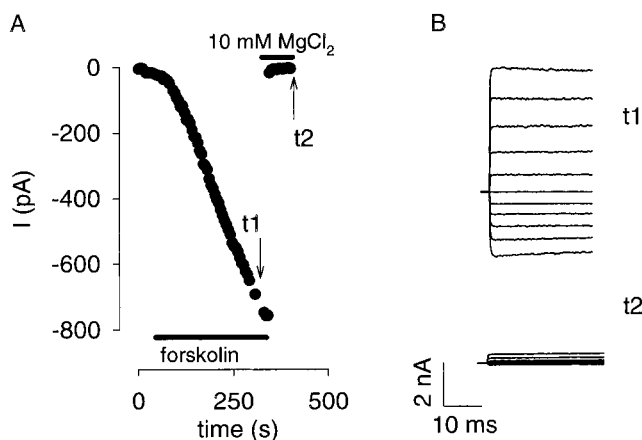

Figure 4. Forskolin-induced currents reflecting cAMP concentration rises at oCNG channels, despite rapid dialysis of the bulk cytosol. (A) Response of an HEK-AC8 cell expressing oCNG channels to 50 μM forskolin in whole-cell configuration, $V_m = -30$ mV. The current reached a plateau in $\sim$300 s. (B) Block of forskolin-induced currents at potentials between $+50$ and -50 mV at times t1 (0.1 mM MgCl$_2$) and t2 (10 mM MgCl$_2$), as indicated in A.

in five of nine cells (Fig. 4 A), consistent with expression in 70% of cells (Fagan et al., 1999). This current was rapidly blocked by 10 mM MgCl$_2$ (Fig. 4 B). No forskolin-induced currents were observed in uninfected cells. We determined that the time needed to exchange the bulk cytoplasm was $\leq$56 s (see below), yet the forskolin-induced currents increased for several minutes at rates similar to those observed in cells studied in the nondialyzed perforated patch configuration. This finding strongly argues that cAMP diffusion from microdomains into the bulk cytosol is impeded. In the next two sections, we show quantitatively that (a) the results cannot be explained if cAMP diffuses freely throughout the cell, and (b) the results can be explained by cell compartment models in which there is a barrier to cAMP diffusion between the microdomains and the bulk cytosol. These models are supported further by experiments in which the flux of cAMP is measured from the whole-cell pipette to the channels.

Free Diffusion of cAMP from Adenylyl Cyclase

In this section, we show that, with no diffusion restriction, cAMP concentrations right next to AC are not

high enough to substantially activate PKA, let alone oCNG channels. Let us consider the local concentration of cAMP near AC. The diffusion equation for constant diffusion coefficient D is written as (Fick, 1855):

$$\frac{\partial C}{\partial t} = D\nabla^2 C, \qquad (1)$$

where C is the concentration of cAMP. If we approximate the AC molecule as a point source on an impermeable plane, Eq. 1 can be solved analytically, yielding (Purves, 1977; Carslaw and Jaeger, 1959; Crank, 1975):

$$C(t, x) = \frac{k_{cat}}{2\pi D x} erfc\left[\frac{x}{(4Dt)^{0.5}}\right], \qquad (2)$$

where k_{cat} is the turnover number, x is the distance from the catalytic site of AC, and t is time. Given that the radius of HEK-AC8 cells is $\sim$10 μm and that we are estimating cAMP concentrations 10 nm (within molecular dimensions) from AC, this geometric approximation is valid. For the simulation, we assumed a diffusion coefficient for cAMP in cytoplasm of 3×10^{-6} cm²/s (Lowe and Gold, 1993; Chen et al., 1999) and a k_{cat} of 59 s^{-1} (Dessauer and Gilman, 1997). Strictly speaking, the value of 59 s^{-1} is the slowest forward first-order rate constant of the model proposed by Dessauer and Gilman (1997), and therefore represents an upper limit for k_{cat}. In fact, a k_{cat} of 12 s^{-1} has been measured for a soluble AC construct (Dessauer and Gilman, 1996). Using Eq. 2, the maximal cAMP concentration 10 nm from AC is 5.2 nM (Fig. 5, A and C). This is considerably lower than the concentration of cAMP required to half-maximally activate either oCNG channels or PKA (Fig. 5 A), clearly demonstrating that, by itself, colocal-

ization of oCNG channels and AC cannot explain the data we have presented.

It is useful to compare this low cAMP concentration with the high concentration of Ca^{2+} reached near the mouth of a Ca^{2+} channel (Fig. 5 B, see legend for details). The high steady state Ca^{2+} concentration near the channel (88 μM at 5 nm) is similar to previous estimates of local Ca^{2+} concentration (Naraghi and Neher, 1997), and is due to the high Ca^{2+} throughput of these channels (5×10^5 s^{-1} for Ca^{2+} channels vs. 59 s^{-1} for AC). In contrast, the slow synthesis rate of cAMP dictates that concentrations of cAMP cannot reach such levels without a diffusional barrier.

With no restriction on diffusion, the steady state cAMP concentration near AC is reached rapidly (within 2 ms, Fig. 5 C). This is much faster than the time course we observed ($\sim$150 s, see Fig. 3). The solution in the experimental chamber was exchanged in $\sim$15 s and forskolin activation of AC occurs within 8 s (Frace et al., 1993). Thus, the time course of cAMP accumulation is likely due to filling of a compartment within the cell.

Cell Compartment Models

Fig. 6 shows a simple compartment model of the cell and whole-cell patch pipette. The cell contains two compartments: a microdomain (compartment 1) in which AC produces cAMP, and the bulk cytosol (compartment 2). The pipette is represented by compartment 3. In simulating the flux of cAMP between the compartments, we have made the following assumptions: (a) diffusion between compartments is restricted by a barrier, and (b) diffusion within each compartment is much more rapid than diffusion between
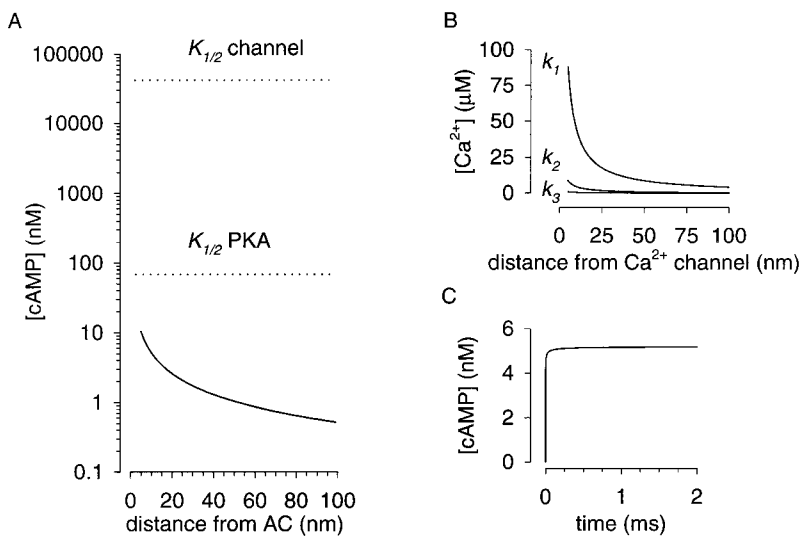

Figure 5. Estimate of second messenger concentrations near their source, assuming free diffusion. (A) Simulation of steady state cAMP concentration near AC, $k_{cat} = 59$ s^{-1} (see text for details). Even as close as 5 nm from AC the cAMP concentration is considerably lower than the concentration required to half-maximally activate PKA, and $\sim$10,000-fold lower than that required to half-maximally activate oCNG channels. (B) The high throughputs of Ca^{2+} channels are responsible for the high Ca^{2+} concentrations near the mouth of the channel. The Ca^{2+} throughputs ($k_1 = 5 \times 10^5$ s^{-1}, $k_2 = 5 \times 10^4$ s^{-1}, and $k_3 = 5 \times 10^3$ s^{-1}) were chosen to represent a physiologic range from the high Ca^{2+} throughput of voltage-gated Ca^{2+} channels (Hille, 1992) to the low Ca^{2+} throughput of I_{CRAC} channels (Zweifach and Lewis, 1993). These results are similar to those of Naraghi and Neher (1997); however, Ca^{2+} buffering was not considered in our simulations. (C) Time course of cAMP accumulation 10 nm from AC. The steady state cAMP concentration is reached within 2 ms. These simulations demonstrate that 2-D localization of AC and oCNG channels is not enough to explain our results.
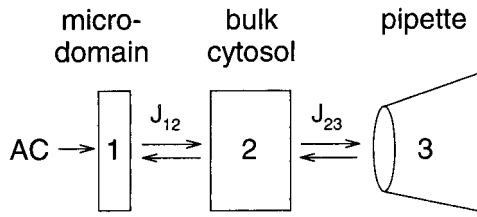
Figure 6. Compartment model used to quantitatively describe the generation of cAMP within microdomains. Details are given in the text.
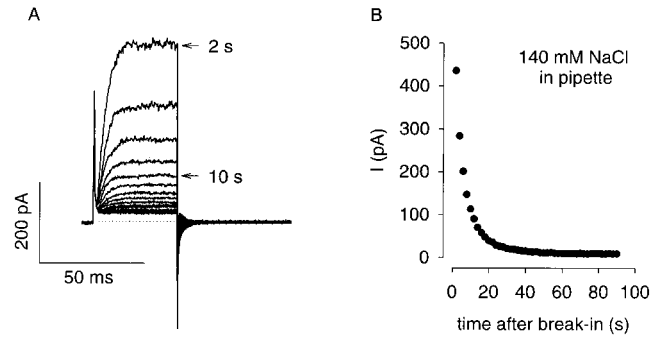

Figure 7. Reduction of voltage-gated K^+ channel current due to wash-in of high-NaCl pipette solution. (A) Currents were elicited every 2 s by 40-ms pulses to $+60$ mV followed by 60-ms pulses to -40 mV. The holding potential was -80 mV. The sweeps at 2 and 10 s after break in are marked. Break in occurred at 0 s. The dotted line represents zero current. No series resistance compensation, capacitance compensation, or leak correction was used. No run down of K^+ currents was observed in control experiments. (B) The steady state current in A is shown as a function of time. Currents were measured between 35 and 40 ms for each trace. The rapid run down of the current indicates that the wash-in of NaCl is fast (90% complete in 20 s for this experiment).

compartments. Thus, the concentration in each compartment is considered to be uniform (rapidly equilibrated) at all times. The second assumption is justified, based on how rapidly cAMP would diffuse without restriction across the entire cell. Using the equation for diffusion in three dimensions: $\langle x^2 \rangle = 6Dt$, cAMP can diffuse across a C6-2B cell ($x = 16.8\ \mu$m) in 160 ms. This is considerably faster than the exchange times between cellular compartments (see below).

This system is described by the following three equations (Eqs. 3–5):

$$\frac{dC_1}{dt} = \frac{J_{12}}{V_1}(C_2 - C_1) \tag{3}$$

$$\frac{dC_2}{dt} = \frac{J_{12}}{V_2}(C_1 - C_2) + \frac{J_{23}}{V_2}(C_3 - C_2) \tag{4}$$

$$\frac{dC_3}{dt} = \frac{J_{23}}{V_3}(C_2 - C_3), \tag{5}$$

where V_1, V_2, and V_3 are the volumes of each compartment, C_1, C_2, and C_3 are the concentrations in each compartment, and J_{12} and J_{23} are flux coefficients between compartments 1 and 2, and compartments 2 and 3, respectively.

Before using this model to simulate the accumulation of cAMP synthesized by AC, we sought to experimentally determine the rates of transfer of material between the compartments in HEK-293 cells. To estimate the rate of transfer between the pipette and the bulk cytosol (compartments 3 and 2), we first measured the reduction in endogenous, voltage-gated K^+ currents in response to the wash-in of a solution containing high NaCl and low KCl (whole-cell pipette 5, Table I). After break-in, currents were measured every 2 s in response to 40-ms pulses to $+60$ mV from a holding potential of -80 mV (Fig. 7). This protocol allowed us to monitor the endogenous K^+ currents without rundown. When the pipette solution contained high NaCl, the amplitude of the outward current decreased rapidly (90% in 22 ± 4 s, $n = 4$). To ensure that the results were not affected significantly by Na^+ block of the K^+ currents, we also examined tail currents at -40 mV and obtained a

similar time course. No reduction of current was observed when the pipette solution contained high KCl (whole-cell pipette 1, Table I). To estimate the rate of transfer of cAMP based on these results, we scaled the wash-in time by the ratio of diffusion coefficients for Na^+ and cAMP (3.5; Pusch and Neher, 1988), yielding a 90% exchange time of 77 s.

To estimate the rate of transfer of cAMP between the cytosol and the microdomain (compartments 2 and 1), we measured the development of currents through oCNG channels in response to the wash-in of 40 μM or 1 mM cAMP from the patch pipette. These experiments were done with high concentrations of two PDE inhibitors in both the bath (low-Mg bath 2, Table I) and the pipette (whole-cell pipette 6 or 7) solutions. The cells were exposed to the bath solution containing PDE inhibitors for >6 min before break in. As before, currents through oCNG channels were verified by Mg^{2+} block (high-Mg bath 2 solution, Table I). Fig. 8 A shows that, after break in with 40 μM cAMP (a half-saturating concentration) in the pipette, a current developed slowly (90% complete in 194 ± 62 s, $n = 5$). This time course was considerably slower than the exchange of the bulk cytosol, and thus represents another clear demonstration of the diffusional barrier between the cytosol and the microdomain. The time course with 1 mM cAMP in the pipette was much faster (90% complete in 38 ± 16 s, $n = 7$), consistent with this being a supersaturating concentration and high concentrations reaching the channel well before exchange was complete (Fig. 8 B). This result also indi-
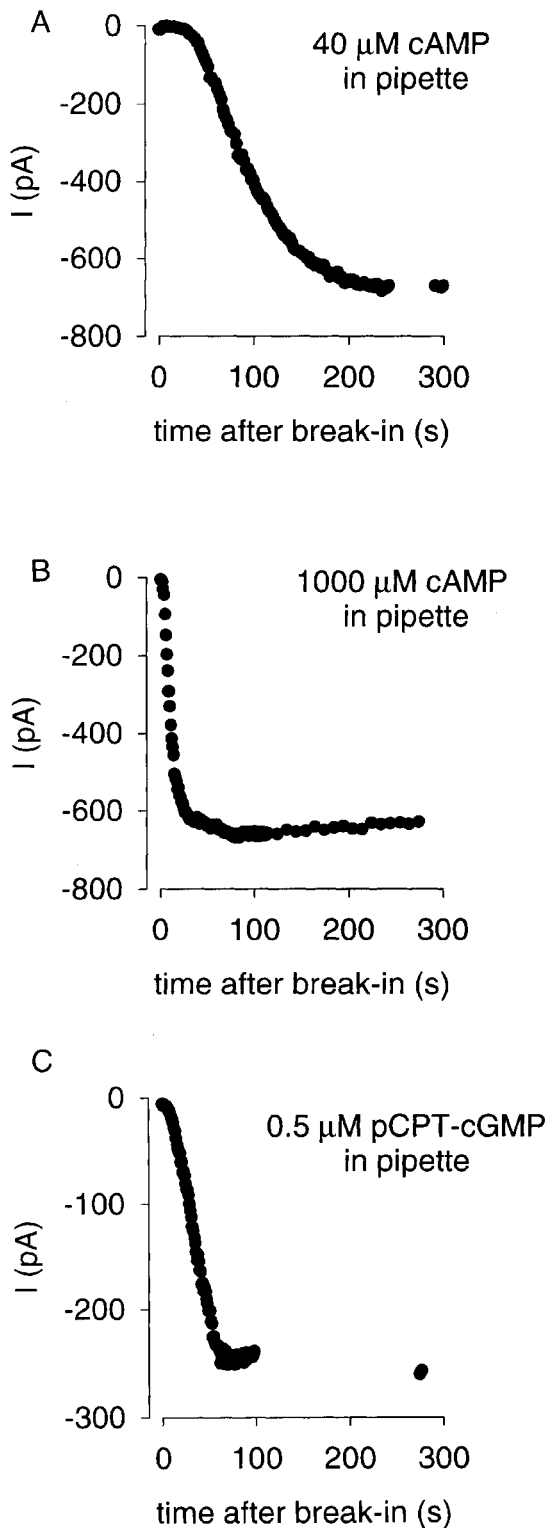
Figure 8. Response of oCNG channels to the wash-in of cyclic nucleotides from the pipette. Currents were measured during 100-ms steps to −50 mV from a holding potential of 0 mV. (A) Wash-in of 40 μM cAMP from the pipette solution. Initially there was a lag followed by a slow, multiexponential increase in current (in this experiment, the current reached 90% of the maximal current in 174 s). Other protocols were run during the brief gap in the data.

cates that cAMP buffering is not the primary restriction on diffusion.[3]

Interestingly, when 0.5 μM pCPT-cGMP (8-*p*-chlorophenylthio-cGMP) was included in the pipette solution (whole-cell pipette 8, Table I), the 90% response time of oCNG channels was 38 ± 18 s, $n = 10$ (Fig. 8 C). This concentration of pCPT-cGMP is 4.5× greater than $K_{1/2}$ (~110 nM), and thus the 90% response time we measured was faster than would be expected at lower pCPT-cGMP concentrations. When this was taken into account, the 90% response time was calculated to be 56 s. The membrane-permeant pCPT-cGMP was apparently able to traverse the barrier between the cytosol and the microdomain more rapidly than cAMP (56 vs. 194 s). Thus, the 56-s wash-in time of pCPT-cGMP can be considered an upper limit for the 90% exchange time between the whole-cell pipette and the bulk cytosol, and was used to constrain J_{23}. The wash-in times for Na^+ and pCPT-cGMP are consistent with those measured in a previous study of chromaffin cells (Pusch and Neher, 1988) and indicate that dialysis of the bulk cytosol is indeed rapid.

We now show that the cell compartment model in Fig. 6 can describe the transfer of cAMP between compartments, the high local and low cytosolic cAMP following AC activation, and the accumulation of cAMP despite rapid dialysis of the cytosol. We used a cytosolic volume of 2.5 pl (based on a cell radius of 8.4 μm), and assumed the volume of the microdomain is 0.04 pl (<2% of the cell volume). Values for the flux coefficients J_{12} and J_{23} of 8.0×10^{-16} liters/s and 9.0×10^{-14} liters/s allowed us to describe the exchange of the bulk cytosol and the wash-in of 40 μM cAMP (for the latter, compare Figs. 9 A and 8

---

[3]These results also serve another important purpose, in that they verify the calibration of the sensor in the whole-cell environment. The time courses of the wash-in of 40 μM and 1 mM cAMP are consistent with a $K_{1/2}$ value for the channels of 40 μM, and inconsistent with $K_{1/2}$ values ≤20 μM. The response to 1 mM cAMP was much faster because high concentrations reached the channel well before the pipette solution equilibrated with the microdomain. If the $K_{1/2}$ were much lower than 40 μM, simulations show that the wash-in of 1 mM cAMP would be considerably faster than 38 s. The flash photolysis experiment in Fig. 1 A is also consistent with $K_{1/2}$ being > 20 μM. The response to a flash was much larger than the response to 20 μM cAMP (added to the patch pipette). These experiments reinforce the conclusion that high local concentrations of cAMP were generated in response to forskolin stimulation.

The points following the gap clearly demonstrate that the current had indeed reached a plateau. (B) Wash-in of 1,000 μM cAMP from the patch pipette. Here the lag was very brief and the increase in current rapid (in this experiment, the current reached 90% of the maximal current in 28 s). (C) Wash-in of 0.5 μM 8-*p*-chlorophenylthio-cGMP from the patch pipette. Interestingly, there was only a small lag and the current increased quickly (in this experiment, the current reached 90% of its maximal value in 48 s). The points following the gap in the data (during which other protocols were run) demonstrate that the current had reached a steady plateau.

A). The 40 μM cAMP time course is dominated by the slow exchange between the cytosol and microdomain, but the finite exchange time between the pipette and cytosol, and the nonlinear response of oCNG channels to cAMP, contribute to the sigmoidal shape. Using the same parameters, we are able to describe the wash-in of 1 mM cAMP (Fig. 9 B).[3] Assuming that there are 450 ACs (each with a k_{cat} of 59 s^{-1}), we can also account for the buildup of high concentrations of cAMP in the microdomain (Fig. 9 C), the accumulation of low concentrations in the bulk cytosol (Fig. 9 C), and the negligible effect of rapid dialysis of the cytosol on the cAMP buildup within the microdomain (Fig. 9 D). We have not attempted to model the lag that is due to (a) the perfusion time ($\sim$15 s), (b) the time it takes forskolin to cross the membrane ($\sim$8 s; Frace et al., 1993), and (c) the detection limit of the channel. Also, we have not included PDE activity in the model. At these levels of forskolin stimulation, the PDE inhibitor 3-isobutyl-1-methylxanthine shortens the lag but does not appreciably change the maximal cAMP concentration reached (data not shown). This is because the cAMP concentration quickly exceeds the K_m of PDE ($\sim$2 μM). In the absence of the microdomain, the same AC activity would generate 5.3 μM cAMP in the cytosol in 300 s (Fig. 9 E), and only 490 nM when the cytosol is being rapidly dialyzed (Fig. 9 F). These concentrations would not appreciably activate oCNG channels. Moreover, 25,000 ACs would be required to generate $\sim$25 μM cAMP if the cytosol were being rapidly dialyzed. This is extremely unlikely for two reasons: (a) that number of ACs would generate almost 300 μM cAMP in an intact cell and (b) the steady state concentration would be reached too quickly (compare Figs. 4 A and 9 F). Thus, the need for microdomains is clear.

Assuming that the flux can be described by simple diffusion, the flux coefficient is related to the classically defined quantities permeability (p) and diffusion coefficient (D) by the relations $J = P \cdot A = D \cdot A/l$, where A is the cross-sectional area and l is the thickness of the barrier. The flux coefficient between the whole-cell pipette and the cytosol ($J_{23} = 9.0 \times 10^{-14}$ liters/s) can be explained by a diffusion coefficient of 3×10^{-6} cm^2/s (the cytosolic diffusion coefficient of cAMP), a barrier thickness of 1 μm, and a cross-sectional area of 0.3 μm^2. The flux coefficient between the microdomain and the cytosol ($J_{12} = 8.0 \times 10^{-16}$ liters/s) can be better understood by examining the following cases. If the cross-sectional area is the entire surface area of the cell (890 μm^2), and the barrier thickness is 1 μm, then J_{12} can be explained by an effective diffusion coefficient of 9.1×10^{-13} cm^2/s. If, instead, the diffusion coefficient is 3×10^{-6} cm^2/s and the barrier thickness is 1 μm, then J_{12} can be explained by a cross-sectional area of 2.7×10^{-3} μm^2. It is likely that the barrier consists of both a reduced diffusion coefficient and a cross-sectional area smaller than the entire surface area of the cell. For example, if each one is reduced by the same factor (576), then J_{12} can be explained by an effective diffusion coefficient of 5.2×10^{-9} cm^2/s and a cross-sectional area of 1.5 μm^2. A challenge for the future is to determine the size of the microdomains and the exact nature of the permeability barriers.

DISCUSSION

The use of oCNG channels as cAMP sensors has allowed the first real-time, localized measurement of cAMP concentration in single cells. By comparing local and global measures of cAMP accumulation, we conclude that the diffusion of cAMP from the subcellular compartments where it is produced is hindered. This conclusion is reinforced by the observation that forskolin-induced cAMP production can be detected in the rapidly dialyzed, whole-cell configuration. These results are easily described by a three-compartment model (microdomain, cytosol, whole-cell pipette) in which the transfer rates between compartments were determined in independent experiments.

The Advantages of oCNG Channels as cAMP Sensors

We have demonstrated here that oCNG channels give a higher resolution view of cAMP signaling than other available methods. In this paper, we have taken advantage of several of the unique features of oCNG channels: membrane localization, accurate calibration, dynamic range, and lack of desensitization. Moreover, we found that these channels colocalize with AC in discrete regions of the surface membrane, which makes them ideal for studying cAMP signals near their point of generation. The channels also have rapid gating kinetics and, although we have not yet taken advantage of it, this feature will be very useful in studying the kinetics of AC regulation and the dynamics of cAMP signals.

Another way to use oCNG channels as cAMP sensors is to measure Ca^{2+} influx with optical methods. This would allow the measurement of localized cAMP signals in cells or cellular regions where electrical recording is difficult. For example, localized second messenger signaling has been identified in dendritic spines (Mons et al., 1995; Finch and Augustine, 1998; Takechi et al., 1998). Ca^{2+} influx through homomultimeric oCNG channels has been measured previously (Frings et al., 1995). To determine whether Ca^{2+} permeability of the channel can be used to detect cAMP produced by AC, we examined the forskolin dose dependence of Ca^{2+} influx in populations of HEK-AC8 cells. In cells expressing oCNG channels, a forskolin dose-dependent increase in intracellular Ca^{2+} concentration was observed (Fig. 10 A). Uninfected cells showed little increase in intracellular Ca^{2+} concentration in response to forskolin (Fig. 10 B). These results clearly demonstrate that AC activity can be monitored using Ca^{2+} influx through oCNG channels.
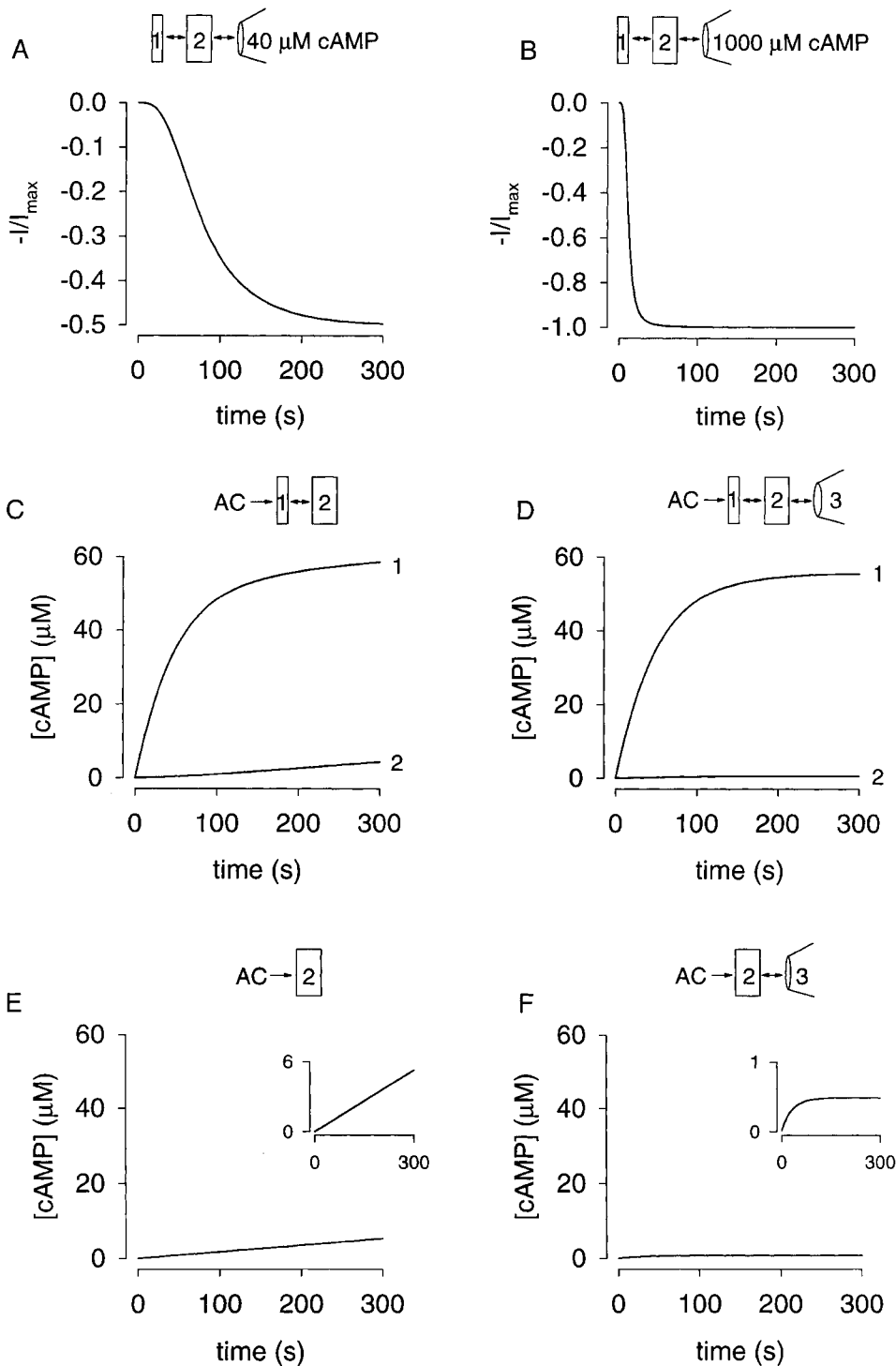
Figure 9. Simulations of data presented in this paper using the compartment model. The experimental configuration is depicted in each panel. The details of the model are given in the text. The simulations in A and B modeled the responses of oCNG channels within the microdomain using the Hill equation (Fig. 2, legend) with $K_{1/2} = 40$ μM and $N = 2.1$. In C–F, cAMP concentrations were simulated. The simulations in A, B, D, and F used a pipette volume, V_3, of 10 μl; however, because V_3 is large compared with the bulk cytosol or the microdomain, the simulations were insensitive to this value. (A) Wash-in of 40 μM cAMP. The data in Fig. 8, A and C, were used to constrain the simulation (details given in text). These same parameters were used to simulate all of the other data. (B) Wash-in of 1,000 μM cAMP. This simulation accurately describes the response of oCNG channels to wash-in of 1,000 μM cAMP (compare with Fig. 8 B). (C) Simulation of cAMP accumulation in compartments 1 and 2. AC produces cAMP in the microdomain (compartment 1). Cyclic AMP levels within the microdomain reach levels >50 μM (compare with Fig. 3, C and E); cAMP levels in the cytosol (compartment 2) reach ~4 μM, consistent with previous reports measuring cytosolic cAMP levels in response to 50 μM forskolin. (D) Simulation of cAMP accumulation in compartments 1–3. In the microdomain, the cAMP concentration reaches high enough levels (almost as high as in C) to significantly activate oCNG channels. (E) Accumulation of cAMP in compartment 2. Without a microdomain, cAMP levels increase in a linear fashion as the entire cell fills with cAMP. (F) Accumulation of cAMP in compartments 2 and 3. With rapid dialysis by the patch pipette, only small concentrations of cAMP accumulate within the cytosol. These concentrations would not significantly activate oCNG channels. If there were enough AC molecules in these cells (~25,000) to significantly activate oCNG channels in the whole-cell configuration, intact cells would generate almost 300 μM cAMP.

Three-Dimensional Signaling Domains for cAMP

Previous studies have shown that elements of G protein signaling complexes localize within distinct subdomains of the surface membrane (e.g., caveolae; Huang et al., 1997; Okamoto et al., 1998). This implies a 2-D restriction on protein movement within the membrane. However, as shown above, colocalization of oCNG channels and AC is not enough to explain our
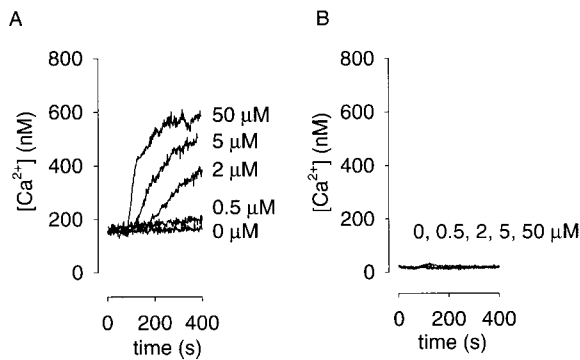
Figure 10. Forskolin-induced Ca^{2+} rises detected in HEK-AC8 cells. (A) Cells expressing oCNG channels. Ca^{2+} influx of 3×10^6 cells in a cuvette in response to increasing forskolin concentrations, as indicated, applied at 60 s. Both the delay and the rate of Ca^{2+} influx were forskolin-concentration dependent. (B) Little or no forskolin-induced response was observed in uninfected cells.

data. The data suggest a 3-D barrier to cAMP diffusion in addition to a 2-D colocalization of membrane proteins. Another study has shown that cAMP is excluded from a portion of a cell by PDE activity (Jurevicius and Fischmeister, 1996). However, PDEs can only lower the concentration of cAMP and therefore cannot account for the high concentrations of cAMP detected by oCNG channels. There is evidence suggesting that the endoplasmic reticulum comes in close contact with the plasma membrane (Finch and Augustine, 1998; Takechi et al., 1998; Patterson et al., 1999; Ma et al., 2000). It is interesting to speculate that endoplasmic reticulum and caveolae form the barrier that hinders the diffusion of cAMP into other regions of the cell (Fig. 11).

The domains of restricted cAMP diffusion may explain our previous results, which demonstrated that local Ca^{2+} rises regulate AC activity, whereas global Ca^{2+} rises have little influence on AC activity (Fagan et al., 1998, 1999). In the latter case, Ca^{2+} may be excluded from the microdomain, or may not reach a sufficient concentration to regulate AC. It is also likely that Ca^{2+} buffering mechanisms contribute to these differences. It is important to note that although buffering of Ca^{2+} or cAMP can slow diffusion, and thus isolate signals into subcellular compartments, buffering cannot significantly increase free concentrations of either second messenger. Overall, the physical and biochemical nature of the microdomains, and how they affect the distribution of Ca^{2+}, remain to be determined.

Physiological Implications of Diffusionally Restricted Microdomains

The hindered diffusion of both Ca^{2+} and cAMP from these microdomains may play important roles in the regulation of cAMP signaling. Such regions may speed

localized cAMP signaling through PKA. A-kinase anchoring proteins (AKAPs) target PKA to specific subcellular regions, and thus facilitate PKA modulation of particular proteins (Gray et al., 1998). Yet to activate PKA half-maximally, cAMP levels must reach >70 nM (Adams et al., 1991). We have shown here that, without hindered diffusion, cAMP does not reach levels high enough to regulate PKA, even near AC. In other words, if diffusionally restricted microdomains did not exist, cAMP levels throughout the cell would have to increase enough to activate PKA. To inactivate PKA, cAMP throughout the cell would then have to be hydrolyzed by phosphodiesterase or extruded. Not only would this process require excessive amounts of energy, it would be slow. Furthermore, PKA would be activated in all subdomains of the cell, and thus many of the advantages of AKAPs would be lost. Based on our results, a more likely scenario is that cAMP is regulated within microdomains, allowing for rapid, local control of PKA activity (Fig. 11 A). In fact, given the maximal rates of cAMP production measured by oCNG channels (HEK-AC8, 0.37 ± 0.09 μM/s; C6-2B, 0.23 ± 0.06 μM/s), PKA within a microdomain would be maximally activated in <1 s. In this model, activation of PKA subunits targeted to different microdomains could occur. For example, it has been shown recently that tethering PKA to the surface membrane with AKAPs enhances the transcription of cAMP-induced genes in PC-12 cells (Cassano et al., 1999). In contrast to membrane-localized PKA, cytosolic PKA would be activated more slowly, by persistent stimulation of AC (Fig. 11 B), as measured in studies using microinjected, fluorescently labeled PKA subunits (Adams et al., 1991, 1993; DeBernardi and Brooker, 1996).

These microdomains may also allow for local and precise feedback control of AC. CNG channels could play a role here. Our findings that they functionally colocalize with Ca^{2+}-stimulable AC (type 8 in HEK-AC8 cells) and Ca^{2+}-inhibitable AC (type 6 in C6-2B cells) suggest that Ca^{2+} influx through these channels provides rapid stimulatory or inhibitory feedback to AC. This may be an important function of CNG channels in nonsensory cells. In this vein, the low apparent cAMP affinities of CNG channels might be explained if they reside primarily in microdomains, where high concentrations can build up. In addition to Ca^{2+} influx through CNG channels, PKA stimulation of Ca^{2+} channel activity could also provide feedback regulation of AC. Local Ca^{2+} feedback regulation of AC could initiate dynamic fluctuations in cAMP (Cooper et al., 1995, 1998; Bhalla and Iyengar, 1999). Such fluctuations would considerably expand the information content of cAMP signals. In summary, the localized signaling described here may help to explain how cAMP coordinates a large variety of cellular phenomena.

t = 120 s

AC
AKAP
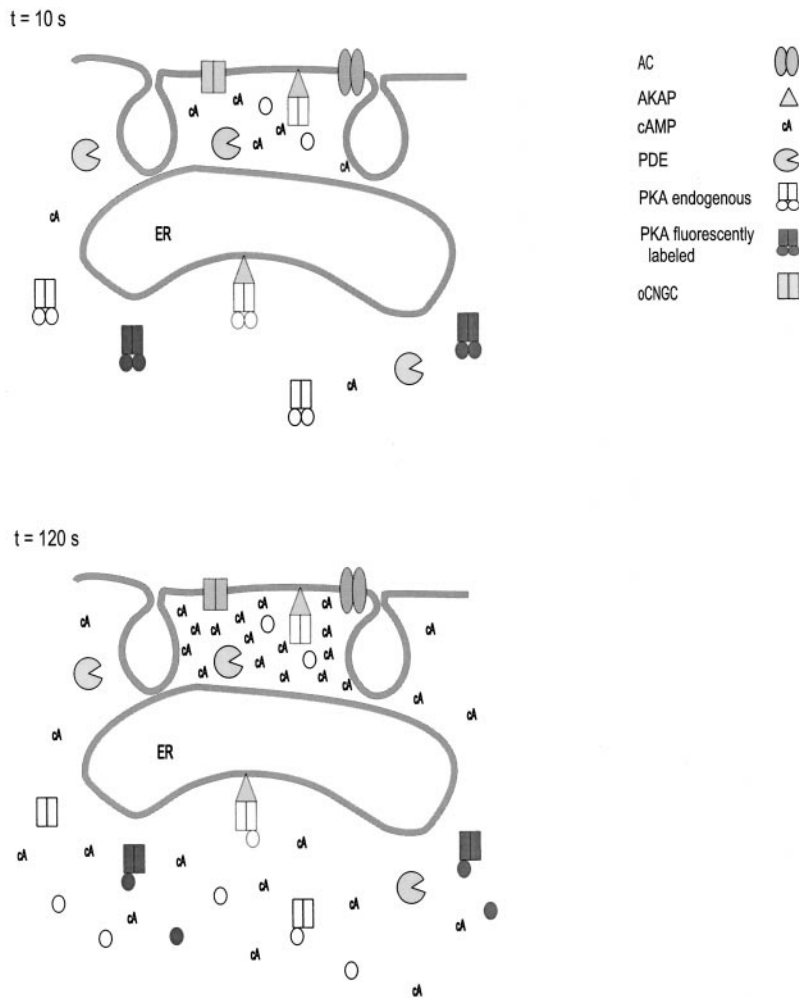cAMP
PDE
PKA endogenous
PKA fluorescently labeled
oCNGC

Figure 11. A model depicting localized signaling by cAMP. Cyclic AMP produced by AC accumulates near the surface membrane, because diffusion is restricted, perhaps by the endoplasmic reticulum (ER) and plasma membrane invaginations such as caveolae. Without such restrictions on diffusion, cAMP molecules would travel across the cell in ~160 ms. Endogenous PKA subunits (regulatory and catalytic subunits depicted as open rectangles and circles) are either diffuse within the cytosol or localized to specific cellular targets by A-kinase anchoring proteins (AKAPs, depicted as triangles). PKA subunits localized within diffusionally restricted microdomains would be rapidly activated after stimulation of AC (A). PKA subunits that are diffuse in the cytosol would be activated more slowly (B), consistent with the data obtained using fluorescently labeled PKA (regulatory and catalytic subunits depicted as filled rectangles and circles; Adams et al., 1991, 1993; DeBernardi and Brooker, 1996, 1998).

REFERENCES

Adams, S., B. Bacskai, A.T. Harootunian, M. Mahaut-Smith, P.J. Sammak, S.S. Taylor, and R.Y. Tsien. 1993. Imaging of cAMP signals and A-kinase translocation in single living cells. *Adv. Second Messenger Phosphoprotein Res.* 28:167–170.

Adams, S.R., A.T. Harootunian, Y.J. Buechler, S.S. Taylor, and R.Y. Tsien. 1991. Fluorescence ratio imaging of cyclic AMP in single cells. *Nature.* 349:694–697.

Allen, M.L., D.S. Koh, and B.L. Tempel. 1998. Cyclic AMP regulates potassium channel expression in C6 glioma by destabilizing Kv1.1 mRNA. *Proc. Natl. Acad. Sci. USA.* 95:7693–7698.

Barber, R., and R.W. Butcher. 1980. The quantitative relationship between intracellular concentration and egress of cyclic AMP from cultured cells. *Mol. Pharmacol.* 19:38–43.

Barovsky, K., C. Pedone, and G. Brooker. 1983. Forskolin-stimulated cyclic AMP accumulation mediates protein synthesis-dependent refractoriness in C6-2B rat glioma cells. *J. Cyclic Nucleotide Res.* 9:181–189.

Baylor, D.A., T.D. Lamb, and K.W. Yau. 1979. Responses of retinal rods to single photons. *J. Physiol.* 288:613–634.

Beavo, J.A. 1995. Cyclic nucleotide phosphodiesterases: functional implications of multiple isoforms. *Physiol. Rev.* 75:725–748.

Bhalla, U.S., and R. Iyengar. 1999. Emergent properties of networks of biological pathways. *Science.* 283:381–387.

Boyajian, C.L., A. Garritsen, and D.M.F. Cooper. 1991. Bradykinin stimulates Ca^{2+} mobilization in NCB-20 cells leading to direct inhibition of adenylyl cyclase. *J. Biol. Chem.* 266:4995–5003.

Cameron, D.A., and E.N. Pugh. 1990. The magnitude, time course and spatial distribution of current induced in salamander rods by cyclic guanine nucleotides. *J. Physiol.* 430:419–439.

Carslaw, H.S., and J.C. Jaeger. 1959. Conduction of Heat in Solids. Clarendon Press, Oxford, UK. 510 pp.

Cassano, S., A. Di Lieto, R. Cerillo, and E.V. Avvedimento. 1999. Membrane-bound cAMP-dependent protein kinase controls cAMP-induced differentiation in PC12 cells. *J. Biol. Chem.* 274:32574–32579.

Chen, C.H., T. Nakamura, and Y. Koutalos. 1999. Cyclic AMP diffusion coefficient in frog olfactory cilia. *Biophys. J.* 76:2861–2867.

Cooper, D.M.F., J.W. Karpen, K.A. Fagan, and N.E. Mons. 1998. Ca^{2+}-sensitive adenylyl cyclases. *Adv. Second Messenger Phosphoprotein Res.* 32:23–51.

Cooper, D.M.F., N. Mons, and J.W. Karpen. 1995. Adenylyl cyclases

and the interaction between calcium and cAMP signalling. *Nature*. 374:421–424.

Crank, J. 1975. The Mathematics of Diffusion. Clarendon Press, Oxford, UK. 414 pp.

DeBernardi, M.A., and G. Brooker. 1996. Single cell Ca^{2+}/cAMP cross-talk monitored by simultaneous Ca^{2+}/cAMP fluorescence ratio imaging. *Proc. Natl. Acad. Sci. USA*. 93:4577–4582.

DeBernardi, M.A., and G. Brooker. 1998. Simultaneous fluorescence ratio imaging of cyclic AMP and calcium kinetics in single living cells. *Adv. Second Messenger Phosphoprotein Res.* 32:195–213.

Debernardi, M.A., R. Munshi, M. Yoshimura, D.M.F. Cooper, and G. Brooker. 1993. Predominant expression of type-VI adenylate cyclase in C6-2B rat glioma cells may account for inhibition of cyclic AMP accumulation by calcium. *Biochem. J.* 293:325–328.

Dessauer, C.W., and A.G. Gilman. 1996. Purification and characterization of a soluble form of mammalian adenylyl cyclase. *J. Biol. Chem.* 271:16967–16974.

Dessauer, C.W., and A.G. Gilman. 1997. The catalytic mechanism of mammalian adenylyl cyclase equilibrium binding and kinetic analysis of P-site inhibition. *J. Biol. Chem.* 272:27787–27795.

Detlev, S., and D. Restrepo. 1998. Transduction mechanisms in vertebrate olfactory receptor cells. *Physiol. Rev.* 78:429–466.

Dhallan, R.S., K.W. Yau, K.A. Schrader, and R.R. Reed. 1990. Primary structure and functional expression of a cyclic nucleotide-activated channel from olfactory neurons. *Nature*. 347:184–187.

Fagan, K.A., N. Mons, and D.M.F. Cooper. 1998. Dependence of the Ca^{2+}-inhibitable adenylyl cyclase of C6-2B glioma cells on capacitative Ca^{2+} entry. *J. Biol. Chem.* 273:9297–9305.

Fagan, K.A., T.C. Rich, S. Tolman, J. Schaack, J.W. Karpen, and D.M.F. Cooper. 1999. Adenovirus-mediated expression of an olfactory cyclic nucleotide–gated channel regulates the endogenous Ca^{2+}-inhibitable adenylyl cyclase in C6-2B glioma cells. *J. Biol. Chem.* 274:12445–12453.

Fick, A. 1855. Ueber diffusion. *Ann. Phys. Chem.* 94:59–86.

Finch, E.A., and G.J. Augustine. 1998. Local calcium signalling by inositol-1,4,5-trisphosphate in Purkinje cell dendrites. *Nature*. 396:753–756.

Finn, J.T., M.E. Grunwald, and K.W. Yau. 1996. Cyclic nucleotide–gated ion channels: an extended family with diverse functions. *Annu. Rev. Physiol.* 58:395–426.

Frace, A.M., P.-F. Mery, R. Fischmeister, and H.C. Hartzell. 1993. Rate-limiting steps in β-adrenergic stimulation of cardiac calcium current. *J. Gen. Physiol.* 101:337–353.

Frings, S., R. Seifert, M. Godde, and U.B. Kaupp. 1995. Profoundly different calcium permeation and blockage determine the specific function of distinct cyclic nucleotide–gated channels. *Neuron*. 15:169–179.

Gold, G.H. 1999. Controversial issues in vertebrate olfactory transduction. *Annu. Rev. Physiol.* 61:857–871.

Gray, P.C., J.D. Scott, and W.A. Catterall. 1998. Regulation of ion channels by cAMP-dependent protein kinase and A-kinase anchoring proteins. *Curr. Opin. Neurobiol.* 8:330–334.

Gray-Keller, M., W. Denk, B. Shraiman, and P.B. Detwiler. 1999. Longitudinal spread of second messenger signals in isolated rod outer segments of lizards. *J. Physiol.* 513:679–692.

Hagen, V., C. Dzeja, S. Frings, J. Bendig, E. Krause, and U.B. Kaupp. 1996. Caged compounds of hydrolysis-resistant analogues of cAMP and cGMP: synthesis and application to cyclic nucleotide–gated channels. *Biochemistry*. 35:7762–7771.

Harootunian, A.T., S.R. Adams, W. Wen, J.L. Meinkoth, S.S. Taylor, and R.Y. Tsien. 1993. Movement of the free catalytic subunit of cAMP-dependent protein kinase into and out of the nucleus can be explained by diffusion. *Mol. Biol. Cell.* 4:993–1002.

Hille, B. 1992. Ionic Channels of Excitable Membranes. 2nd ed. Sinauer Associates, Inc., Sunderland, MA. 607 pp.

Horn, R., and A. Marty. 1988. Muscarinic activation of ionic currents measured by a new whole-cell recording method. *J. Gen. Physiol.* 92:145–159.

Huang, C., J.R. Hepler, L.T. Chen, A.G. Gilman, R.G.W. Anderson, and S.M. Mumby. 1997. Organization of G proteins and adenylyl cyclase at the plasma membrane. *Mol. Biol. Cell.* 8:2365–2378.

Jurevicius, J., and R. Fischmeister. 1996. cAMP compartmentation is responsible for a local activation of cardiac Ca^{2+} channels by β-adrenergic agonists. *Proc. Natl. Acad. Sci. USA*. 93:295–299.

Karpen, J.W., A.L. Zimmerman, L. Stryer, and D.A. Baylor. 1988. Gating kinetics of the cyclic-GMP–activated channel of retinal rods: flash photolysis and voltage-jump studies. *Proc. Natl. Acad. Sci. USA*. 85:1287–1291.

Koutalos, Y., R.L. Brown, J.W. Karpen, and K.W. Yau. 1995a. Diffusion coefficient of the cyclic GMP analog 8-(fluoresceinyl)thioguanosine 3′,5′ cyclic monophosphate in the salamander rod outer segment. *Biophys. J.* 69:2163–2167.

Koutalos, Y., K. Nakatani, and K.-W. Yau. 1995b. Characterization of guanylate cyclase activity in single retinal rod outer segments. *J. Gen. Physiol.* 106:863–890.

Koutalos, Y., K. Nakatani, and K.W. Yau. 1995c. The cGMP-phosphodiesterase and its contribution to sensitivity regulation in retinal rods. *J. Gen. Physiol.* 106:891–921.

Koutalos, Y., K. Nakatani, and K.W. Yau. 1995d. Cyclic GMP diffusion coefficient in rod photoreceptor outer segments. *Biophys. J.* 68:373–382.

Krupinski, J., F. Coussen, H.A. Bakalyar, W.J. Tang, P.G. Feinstein, K. Orth, C. Slaughter, R.R. Reed, and A.G. Gilman. 1989. Adenylyl cyclase amino acid sequence: possible channel- or transporter-like structure. *Science*. 244:1558–1564.

Lagnado, L., and D.A. Baylor. 1992. Signal flow in visual transduction. *Neuron*. 8:995–1002.

Lamb, T.D., P.A. McNaughton, and K.W. Yau. 1981. Spatial spread of activation and background desensitization in toad rod outer segments. *J. Physiol.* 319:463–496.

Levitan, I.B. 1994. Modulation of ion channels by protein phosphorylation and dephosphorylation. *Annu. Rev. Physiol.* 56:193–212.

Liu, M., T.Y. Chen, B. Ahamed, J. Li, and K.W. Yau. 1994. Calcium-calmodulin modulation of the olfactory cyclic nucleotide–gated cation channel. *Science*. 266:1348–1354.

Lowe, G., and G.H. Gold. 1993. Contribution of ciliary cyclic nucleotide–gated conductance to olfactory transduction in the salamander. *J. Physiol.* 462:175–196.

Ma, H.T., R.L. Patterson, D.B. van Rossum, L. Birnbaumer, K. Mikoshiba, and D.L. Gill. 2000. Requirement of the inositol trisphosphate receptor for activation of store-operated Ca^{2+} channels. *Science*. 287:1647–1651.

Molday, R.S. 1998. Photoreceptor membrane proteins, phototransduction, and retinal degenerative diseases: the Friedenwald lecture. *Invest. Opthalmol. Vis. Sci.* 39:2493–2513.

Mons, N., A. Harry, P. Dubourg, R.T. Premont, R. Iyengar, and D.M.F. Cooper. 1995. Immunohistochemical localization of adenylyl cyclase in rat brain indicates a highly selective concentration at synapses. *Proc. Natl. Acad. Sci. USA*. 92:8473–8477.

Montminy, M. 1997. Transcriptional regulation by cyclic AMP. *Annu. Rev. Biochem.* 66:807–822.

Nakatani, K., and K.-W. Yau. 1988. Guanosine 3′,5′-cyclic monophosphate–activated conductance studied in a truncated rod outer segment of the toad. *J. Physiol.* 395:731–753.

Naraghi, M., and E. Neher. 1997. Linearized buffered Ca^{2+} diffusion in microdomains and its implications for calculation of $[Ca^{2+}]$ at the mouth of a calcium channel. *Biophys. J.* 17:6961–6973.

Okamoto, T., A. Schlegel, P.E. Scherer, and M.P. Lisanti. 1998. Caveolins, a family of scaffolding proteins for organizing "preassem-

bled signaling complexes" at the plasma membrane. *J. Biol. Chem.* 273:5419–5422.

Olson, A., and E.N. Pugh. 1993. Diffusion coefficient of cyclic GMP in salamander rod outer segments estimated with two fluorescent probes. *Biophys. J.* 65:1335–1352.

Patterson, R.L., D.B. van Rossum, and D.L. Gill. 1999. Store-operated Ca^{2+} entry: evidence for a secretion-like coupling model. *Cell.* 98:487–499.

Polans, A., W. Baehr, and K. Palczewski. 1996. Turned on by Ca^{2+}! The physiology and pathology of Ca^{2+}-binding proteins in the retina. *Trends Neurosci.* 19:547–554.

Pugh, E.N., T. Duda, A. Sitaramayya, and R.K. Sharma. 1997. Photoreceptor guanylate cyclases: a review. *Biosci. Rep.* 17:429–473.

Pugh, E.N., and T.D. Lamb. 1993. Amplification and kinetics of the activation steps in phototransduction. *Biochim. Biophys. Acta.* 1141:111–149.

Purves, R.D. 1977. The time course of cellular responses to iontophoretically applied drugs. *J. Theor. Biol.* 65:327–344.

Pusch, M., and E. Neher. 1988. Rates of diffusional exchange between small cells and a measuring patch pipette. *Pflügers Arch.* 411:204–211.

Smit, M.J., and R. Iyengar. 1998. Mammalian adenylyl cyclases. *Adv. Second Messenger Phosphoprotein Res.* 32:1–21.

Stryer, L. 1991. Visual excitation and recovery. *J. Biol. Chem.* 266:10711–10714.

Sudlow, L.C., and R. Gillette. 1997. Cyclic AMP levels, adenylyl cyclase activity, and their stimulation by serotonin quantified in intact neurons. *J. Gen. Physiol.* 110:243–255.

Takechi, H., J. Eilers, and A. Konnerth. 1998. A new class of synaptic response involving calcium release in dendritic spines. *Nature.* 396:757–760.

Tian, D., D. Huang, R.C. Brown, and R.A. Jungmann. 1998a. Protein kinase A stimulates binding of multiple proteins to a U-rich domain in the 3′-untranslated region of lactate dehydrogenase A

mRNA that is required for the regulation of mRNA stability. *J. Biol. Chem.* 273:28454–28460.

Tian, D., D. Huang, S. Short, M.L. Short, and R.A. Jungmann. 1998b. Protein kinase A-regulated instability site in the 3′-untranslated region of lactate dehydrogenase-A subunit mRNA. *J. Biol. Chem.* 273:24861–24866.

Trautwein, W., and J. Hescheler. 1990. Regulation of the L-type calcium current by phosphorylation and G proteins. *Annu. Rev. Physiol.* 52:257–274.

Trivedi, B., and R.H. Kramer. 1998. Real-time patch-cram detection of intracellular cGMP reveals long-term suppression of responses to NO and muscarinic agonists. *Neuron.* 21:895–906.

Tsien, R.W. 1983. Calcium channels in excitable cell membranes. *Annu. Rev. Physiol.* 45:341–358.

Wootton, J.F., and D.R. Trentham. 1989. "Caged" compounds to probe the dynamics of cellular processes: synthesis and properties of some novel photosensitive P-2-nitrobenzyl esters of nucleotides. *NATO ASI Ser. Ser. C Math. Phys. Sci.* 272:277–296.

Yarfitz, S., and J.B. Hurley. 1994. Transduction mechanisms of vertebrate and invertebrate photoreceptors. *J. Biol. Chem.* 269:14329–14332.

Yau, K.W. 1994. Phototransduction mechanism in retinal rods and cones: the Friedenwald lecture. *Invest. Ophthalmol. Vis. Sci.* 35:9–32.

Zaccolo, M., F. De Giorgi, C.Y. Cho, L. Feng, T. Knapp, P.A. Negulescu, S.S. Taylor, R.Y. Tsien, and T. Pozzan. 2000. A genetically encoded, fluorescent indicator for cyclic AMP in living cells. *Nat. Cell Biol.* 2:25–29.

Zhou, Z., and E. Neher. 1993. Mobile and immobile calcium buffers in bovine adrenal chromaffin cells. *J. Physiol.* 469:245–273.

Zweifach, A., and R.S. Lewis. 1993. Mitogen-regulated Ca^{2+} current of T lymphocytes is activated by depletion of intracellular Ca^{2+} stores. *Proc. Natl. Acad. Sci. USA.* 90:6295–6299.